IET Microwaves, Antennas & Propagation

Research Article

IET Journals
The Institution of Engineering and Technology

Bandwidth and radiation specifications enhancement of monopole antennas loaded with split ring resonators

ISSN 1751-8725
Received on 20th December 2014
Revised on 25th April 2015
Accepted on 20th May 2015
doi: 10.1049/iet-map.2015.0172
www.ietdl.org

Mohammad Alibakhshi-Kenari[1] ✉, *Mohammad Naser-Moghadasi*[1], *R.A. Sadeghzadeh*[2]

[1]*Faculty of Engineering, Science and Research Branch, Islamic Azad University, Tehran, Iran*
[2]*Faculty of Electrical and Computer Engineering, K. N. Toosi University of Technology, Tehran, Iran*
✉ *E-mail: makenari@mtu.edu*

Abstract: New broadband antennas loaded with split ring resonators (SRR) are proposed and investigated. The results illustrate that by loading the conventional monopole antennas with an asymmetrical meander lines SRR, a lower resonance frequency mode can be excited. The dimensions of the SRR have been selected to provide a resonance close the resonance of the monopole antennas. The results illustrate that when both resonance coincide the antennas bandwidths and radiation properties can be enhanced. The length and width of the antennas are $25 \times 10^{-2}\lambda_0 \times 11 \times 10^{-2}\lambda_0$ and $25 \times 10^{-2}\lambda_0 \times 21 \times 10^{-2}\lambda_0$ at 4 GHz for monopole antennas, and $29 \times 10^{-2}\lambda_0 \times 21 \times 10^{-2}\lambda_0$ at 2.9 GHz for both monopole antennas loaded with SRR. For antennas without SRR loading, maximum of measured gains and efficiencies are 3.6 dBi and 78.5% for F-antenna, and 3.9 dBi and 80.2% for T-antenna, hence they appear at 5 GHz. For antennas with SRR loading, these parameters are 4 dBi and 81.2% for F-antenna, and 4.4 dBi and ~83% for T-antenna, which appeared at 6 GHz. By implementing the meander lines SRR as a matching load on the monopole antennas, the resulted antennas cover the measured frequency bandwidths of 2.9–6.41 GHz and 2.6–6.6 GHz (75.4 and ~87% fractional bandwidths), which are ~2.4 and 2.11 times more than monopole antennas with an approximately same in size.

1 Introduction

With the recent developments in wireless telecommunications, devices are becoming smaller and supporting multiple operations. Some portable devices such as smart phones are designed with built in applications to handle numerous voice and data services [1–5]. Therefore, broadband antennas with good radiation characteristics are needed to satisfy the growing need of wireless telecommunication demands [6, 7].

The concept of metamaterial (MTM) has been widely used to improve the characteristics of antennas [8, 9]. Depending on the design requirements, the MTMs can be designed by using the resonant and non-resonant approaches [10–12]. The resonant approach involves the use of resonant inclusions such as split ring resonators (SRRs), complementary SRRs (CSRRs), electric-field coupled-LC, etc. to design the left handed material [13, 14]. Due to the extraordinary properties of the resonant inclusions, the MTMs are widely used to design antennas with improved performances [15, 16]. However it is worth noting that, the resonant inclusions are narrow band naturally due to the resonant requirements to operate near resonant frequency. Therefore, they should be properly integrated with some existing design techniques for improving the performances [7–15].

Recently, a number of studies to improve the bandwidth of the MTM antennas have been reported [17–22]. In this paper, four antennas with and without applying the asymmetrical meander lines SRR loading are presented and demonstrated. The first versions of antennas comprise a monopole radiator without SRR loading and the second versions of them comprise two monopoles with SRR loading. In effect, with implementing the SRR, the second versions bandwidths improve from 31.5 75.4% for F-antenna and from 41.16 to 86.9% for T-antenna, (standing wave ratio [SWR] ≤ 2). Therefore, the SRR loading pull down the resonant frequency, so that it is possible to cover the required frequency ranges related to worldwide interoperability for microwave access (WiMAX-3.5/5.5 GHz) and wireless local area network (WLAN-5.2/5.8 GHz) bands by the second versions of antennas.

This paper is organised as follows. The design procedures are discussed in Section 2. The first part of this section is related to designing the monopole antennas without the asymmetrical meander lines SRR loading and in the second part, the antennas with the asymmetrical meander lines SRR loading are fabricated and tested. Section 3 provides the antennas results, so that an investigation on behaviour of asymmetrical meander lines SRR loaded on both proposed antennas is explained in Section 4. Finally, the conclusions are presented in Section 5.

2 Design process of the proposed antennas

Two antennas with different configurations are proposed (Figs. 1 and 2). The first antenna with F-shaped structure is a conventional monopole antenna without/with using the asymmetrical meander lines SRR loading, and the second antenna with T-shaped configuration is a monopole antenna loaded/unloaded with SRR loading. To validate the designs, both structures are modelled and designed by applying Ansoft's (threedimensional) 3D full-wave electromagnetic field software called to high frequency structure simulator (HFSS) [23] and after optimisation and regulation procedures, the resulted structures were tooled, fabricated, and tested using a network analyser. The constructional elements of the antennas are carved on the Rogers_RT_Duroid5880 substrate with permittivity of $\varepsilon_r = 2.2$, $\tan\delta = 0.002$ and substrate thickness of $h = 0.8$ mm. In these designs, the rectangular slots on an asymmetrical ground plane along with the gap slits on the monopole radiators are used for impedance matching. In addition, in the second versions, a SRR loading is applied for improving the antenna performances.

2.1 F and T-shaped antennas without asymmetrical meander lines SRR loading

Photographs of these antennas with F- and T-shaped configurations are shown in Fig. 1.

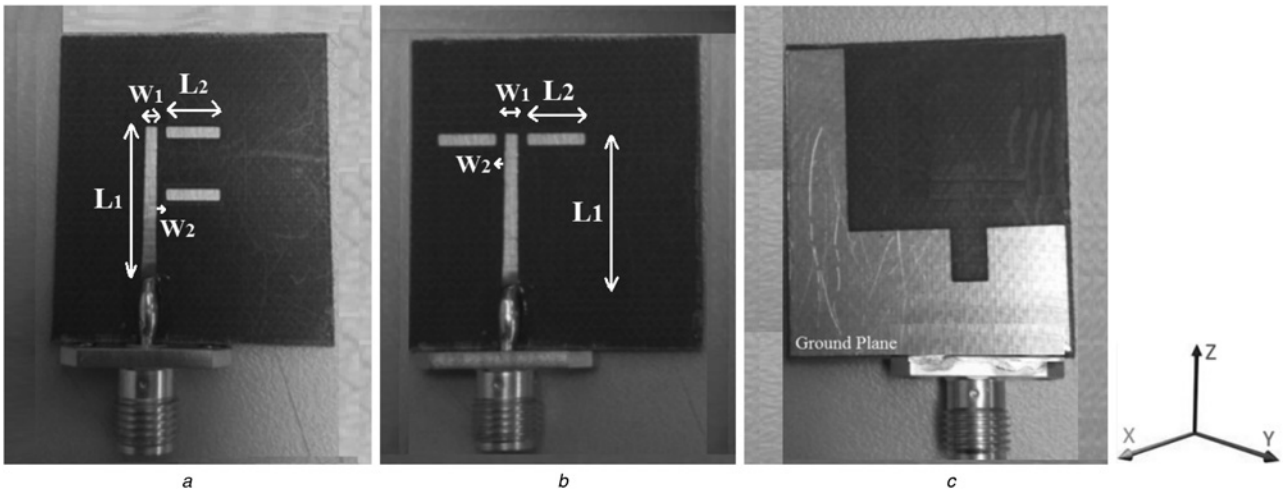

Fig. 1 *Fabricated prototypes of the monopole antennas*

a Top view of F-shaped antenna
b Top view of T-shaped antenna
c Back view of both antennas without SRR loading. Antennas design parameters are $L_1 = 19$ mm, $L_2 = 7$ mm, $W_1 = 1.4$ mm and $W_2 = 0.4$ mm. The antennas are in the XZ plane

These antennas integrate three rectangular radiation patches that are vertically and horizontally arranged, thus creating the F- and T-shaped structures. In these structures, two slits on the monopole radiators along with an asymmetrical feeding with respect to the ground planes are used for impedance matching. The antennas overall sizes are $25 \times 10^{-2}\lambda_0 \times 11 \times 10^{-2}\lambda_0 \times 2 \times 10^{-2}\lambda_0$ for F-antenna and $25 \times 10^{-2}\lambda_0 \times 21 \times 10^{-2}\lambda_0 \times 2 \times 10^{-2}\lambda_0$ for T-antenna, in terms of free space wavelengths (λ_0) at 4 GHz for both monopole antennas and their reflection coefficients are SWR ≤ 2 (Figs. 3 and 4). Regarding with widths of antennas, for implementing T-antenna the designers have coupled and fed this structure by an additional monopole radiator on the other side (Fig. 1*b*). As a result, width of this antenna has slightly extended than F-antenna.

2.2 Proposed antennas loaded with SRR

In this section, previous structures with three rectangular radiation patches to form F and T shapes are extended for presenting better performances. Like the first versions, for matching process, the slits are used on the monopole radiators, and the feed of monopole antennas are asymmetric with respect to the ground planes. For providing better performances compared with previous versions the SRR loading are implemented. This loading excites a lower resonance frequency mode that matches with the resonance frequency of monopole antennas, thus increasing the antennas bandwidths. As a result, the second versions with the asymmetrical meander lines SRR loading can be applicable for the WiMAX (3.5–5.5 GHz) and WLAN (5.2–5.8 GHz) bands. The fabricated prototypes of these antennas with F- and T-shaped configurations and the SRR placed on the ground planes are shown in Fig. 2.

Layout of the fabricated SRR loaded antennas structures drawn to scale. SRR dimensions included, *number* of *SRR pairs* $n = 4$, length of SRR $L_{SRR} = 12$ mm, width of SRR $W_{SRR} = 0.4$ mm and variable distances between SRR pairs $0.4\text{ mm} < D_{SRR} < 0.8$ mm ($D_{Min.} = 0.4$ mm and $D_{Max.} = 0.8$ mm). Adjacent ring pairs are separated $d = 1.5$ mm. The lengths and width of strip are $L_1 = 30$ mm, $L_2 = 11$ mm and $W = 22$ mm, respectively. Too, length and width of slot are $L_S = 3.5$ mm and $W_S = 2.2$ mm, respectively. The structure has been fabricated on a Rogers_RT_Duroid5880 substrate with permittivity of $\varepsilon_r = 2.2$, $\tan\delta = 0.002$ and substrate thickness of $h = 0.8$ mm. Actual devices length and width (including access lines)

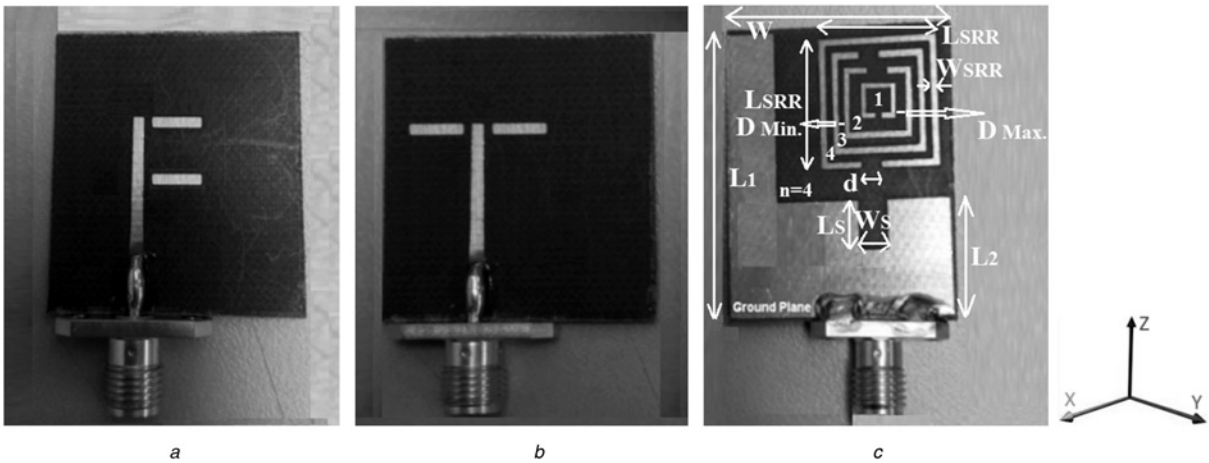

Fig. 2 *Fabricated prototypes of the antennas with asymmetrical meander lines SRR loading*

a Top view of F-shaped antenna
b Top view of T-shaped antenna
c Back view of both antennas with SRR loading. The antennas are in the XZ plane

IET Microw. Antennas Propag., 2015, Vol. 9, Iss. 14, pp. 1487–1496

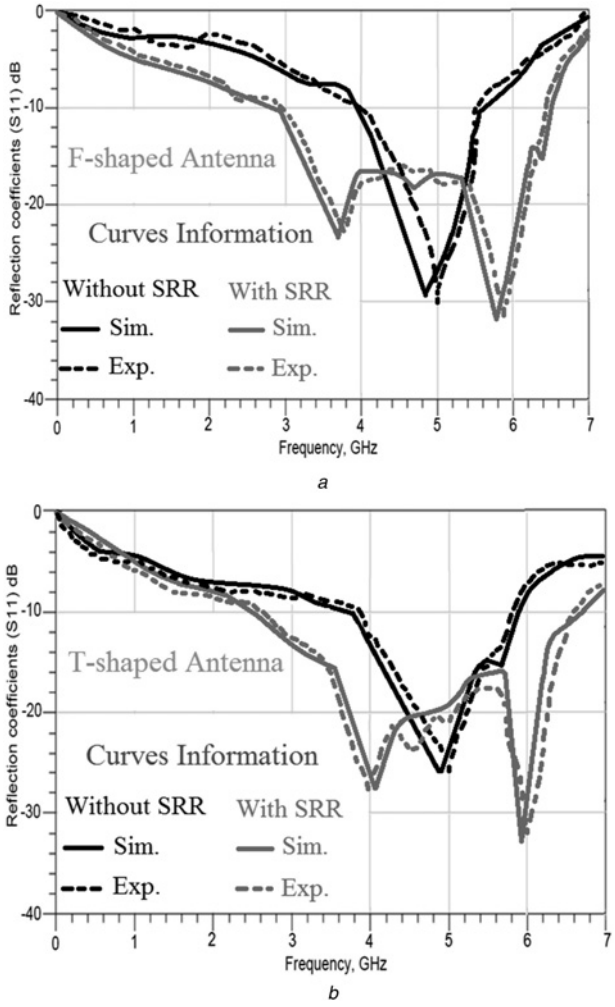

Fig. 3 *Simulated and measured reflection coefficients ($S_{11} < -10$ dB)*

a For F-shaped antenna without/with asymmetrical meander lines SRR loading
b For T-shaped antenna without/with asymmetrical meander lines SRR loading

are 30 mm and 22 mm, respectively. Both antennas have total dimensions of $29 \times 10^{-2}\lambda_0 \times 21 \times 10^{-2}\lambda_0 \times 1 \times 10^{-2}\lambda_0$ at 2.9 GHz and its reflection coefficients are SWR ≤ 2 (Figs. 3 and 4).

3 Results and discussions

In this section a comparison between performances of F and T-antennas without asymmetrical meander lines SRR loading and with this load is provided. The simulated and experimental reflection coefficients ($S_{11} < -10$ dB) of F and T-antennas without/with SRR loading are shown in Figs. 3*a* and *b*, respectively. As clear, F-shaped antenna without meander lines SRR loading covers the impedance bandwidths of 3.95–5.57 GHz (BW = 1.62 GHz) and 4.0–5.50 GHz (BW = 1.5 GHz), which correspond to 34.0 and 31.5% simulated and measured bandwidths. Moreover, the simulated and measured impedance bandwidths for T-antenna without SRR are 3.77–5.85 GHz (BW = 2.08 GHz) and 3.82–5.80 GHz (BW = 1.98 GHz), which correspond to 43.24% and 41.16% operating bandwidths, respectively.

These figures express that with loading SRR on the antennas ground plane, the antennas bandwidths increased to up a considerable ranges. As a result, F-shaped antenna loaded with SRR exhibits 78.27% (2.83–6.47 GHz) frequency bandwidth in simulation by HFSS and 75.40% (2.9–6.41 GHz) measured impedance bandwidth (Fig. 3*a*). Moreover, similar results are obtained by loading meander lines SRR on ground plane of T-shaped antenna. Hence, T-antenna in this case covers the simulated and experimental bandwidths of 2.57–6.68 GHz (4.11 GHz) and 2.6–6.6 GHz (4 GHz), which are corresponded to 88 and ~87% fractional bandwidths, respectively (Fig. 3*b*). According with Figs. 3*a* and *b*, F and T-antennas without SRR have an operating frequency region centred at the frequency of $f_r = 4.80$ and 4.85 GHz from HFSS and both antennas in measurement case resonates at the same frequency of 5 GHz. Moreover it is find that, by loading SRR on the antennas grounds a lower resonance frequency mode for both antennas is excited that matches with the resonance frequency of monopole antennas, thus increasing the antennas bandwidths. F and T-shaped antennas in this case resonates at 3.65 and 5.8 GHz, 4.1 and 5.9 GHz in simulation, and 3.75 and 5.9 GHz, and 4 and 6 GHz in measurement, respectively. Consequently it is found that, the SRR loading extends the impedance bandwidths of monopole antennas for covering the WiMAX (3.5–5.5 GHz) and WLAN (5.2–5.8 GHz) bands. Moreover it is noted of Figs. 3*a* and *b* that, unlike the first versions with measurement bandwidths given by BW = 31.5% (F-antenna) and 41.16% (T-antenna), the second versions have a BW = 75.4% (F-antenna) and 86.9% (T-antenna) which are 2.39 and 2.11 times more. The results demonstrate good agreement between simulations and measurements.

Besides the size and the frequency bandwidth, the radiation properties are main performance parameters in antenna systems. Curves of measured gains and efficiencies versus frequency for the proposed antennas without/with asymmetrical meander lines SRR loading are plotted in Figs. 4*a* and *b*, respectively.

All radiation specifications of the proposed antennas in measurement are listed in Table 1.

Table 1 illustrates that, in case of without SRR loading the peak gain and efficiency occur at 5 GHz for both antennas, which are

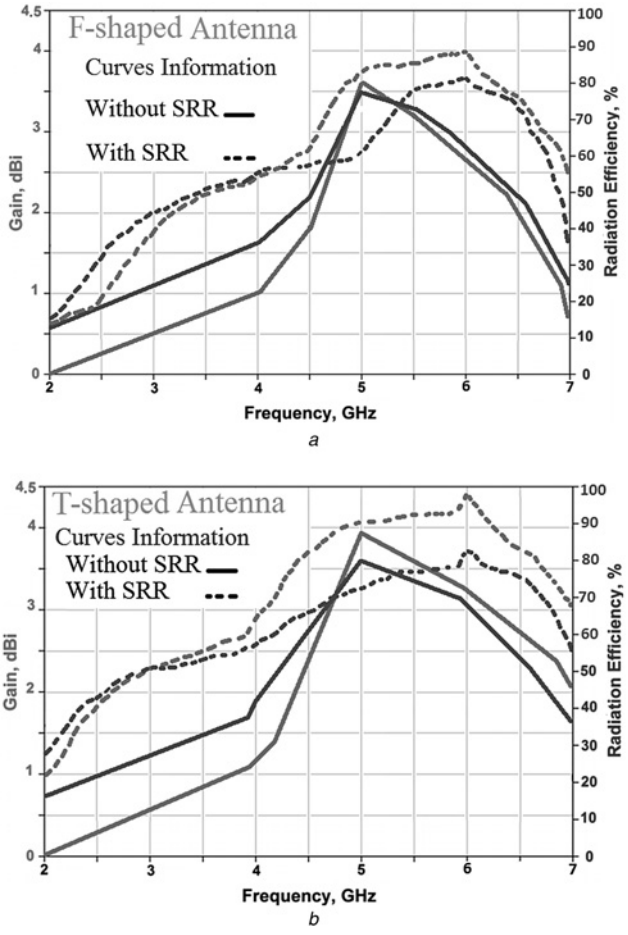

Fig. 4 *Experimental gains and efficiencies curves against frequency*

a For F-antenna without/with SRR loading
b For T-antenna without/with SRR loading

Table 1 Radiation characteristics of the proposed antennas

		Radiation specifications: gain (dBi) and efficiency (%). Maximum values are bold	
		Without asymmetrical meander lines SRR loading	With asym. meander line SRR loading
F-antenna	gain	@ 4, 4.5, **5**, 5.5 GHz: 1, 1.8, **3.6** and 3.2	@ 2.9, 3.8, 5, **6**, 6.41 GHz: 1.7, 2.4, 3.7, **4**, 3.45
	efficiency	@ same Freq.: 36.3, 48.1, **78.5**, 73.8	@ same Freq.: 43.6, 51.7, 60.9, **81.2**, 76.5
T-antenna	gain	@ 3.82, 4, **5**, 5.8 GHz: 1.15, 1.3, **3.9**, 3.3	@ 2.6, 3.82, 4, 5.8, **6**, 6.6 GHz: 1.8, 2.75, 2.9, 4.25, **4.4**, 3.7
	efficiency	@ same Freq.: 36.5, 42.1, **80.2**, 70.4	@ same Freq.: 45.5, 56.5, 58.9, 79.3, **82.6**, 75.4

3.6 dBi and 78.5% for F-antenna and 3.9 dBi and 80.2% for T-antenna, (Figs. 4*a* and *b*). Moreover, minimum values of these parameters are 1.0 dBi and 36.3% for F-antenna and 1.15 dBi and 36.5 for T-antenna occurred at 4.00 and 3.82 GHz, respectively. In the opposite case (designed by meander lines SRR), the maximum gain and efficiency for both antennas happened at 6 GHz are 4 dBi and 81.2% for F-antenna and 4.4 dBi and 82.6% for T-antenna. So that minimum amounts of these parameters are 1.7 dBi and 43.6% occurred at 2.9 GHz for F-antenna and 1.8 dBi and 45.5% happened at 2.6 GHz for T-antenna.

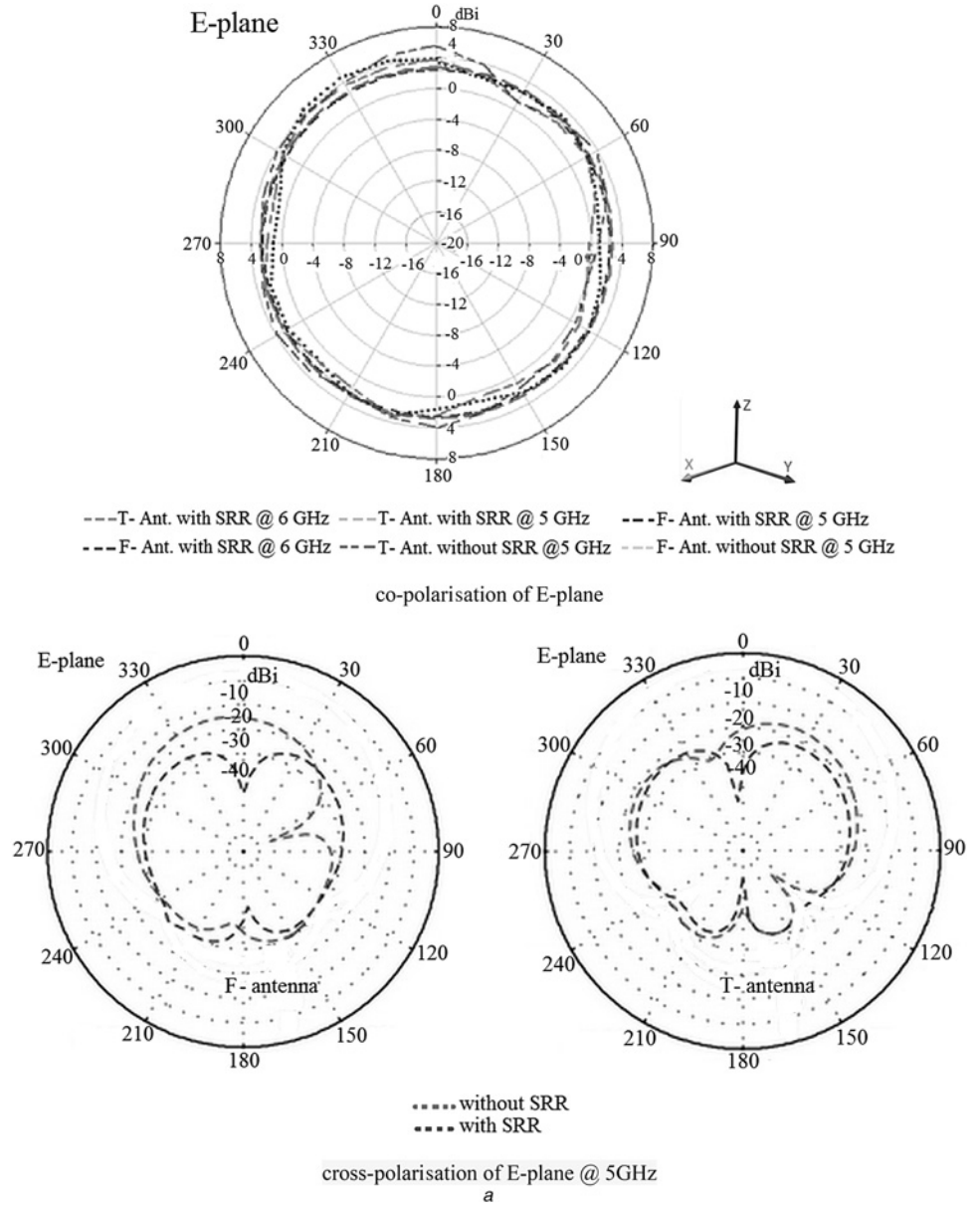

Fig. 5 *a–b Measured E and H-planes radiation patterns for proposed antennas without/with asymmetrical meander lines SRR loading at the operating frequencies. c–d Current distributions of the F- and T-antennas without/with SRR loading at resonance frequencies*

a Experimental E-plane radiation patterns for F- and T-shaped antenna. E-plane corresponds to Phi = 0°
b Experimental H-plane radiation patterns for F and T-shaped antenna. H-plane corresponds to Theta = 90°. The slight shift in beam direction in H-plane is due to loading of SRR on the ground plane
c Without SRR loading
d Loaded with SRR

IET Microw. Antennas Propag., 2015, Vol. 9, Iss. 14, pp. 1487–1496

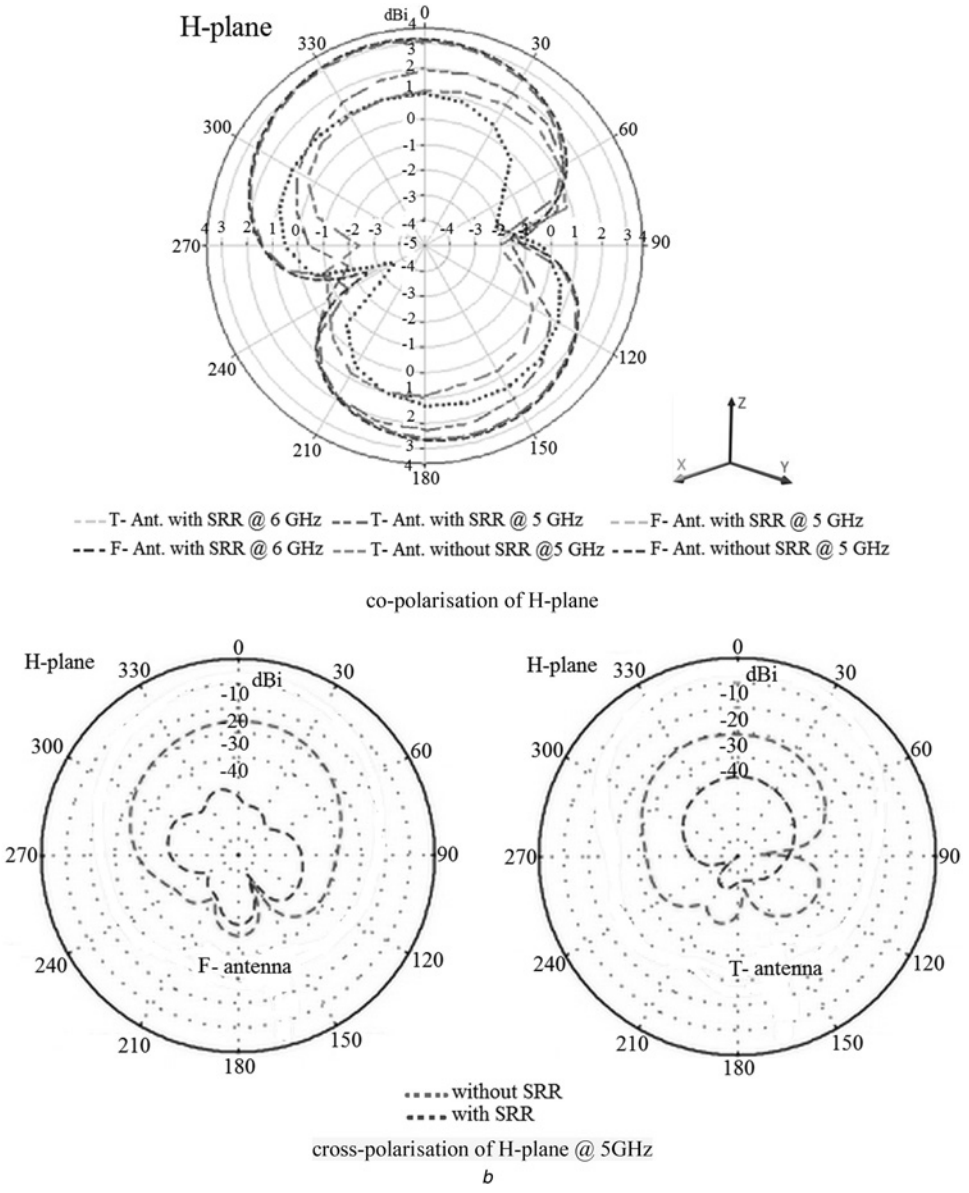

b

Fig. 5 *Continued*

The measured E and H-planes radiation patterns for both proposed antennas without/with asymmetrical meander lines SRR loading at the operating frequencies are displayed in Figs. 5*a* and *b*, respectively.

The omni-directional radiation patterns are obtained for E-plane at all operating frequencies in both cases of without and with SRR loading (Fig. 5*a*). While, the radiation patterns for H-plane at all operating frequencies have the bidirectional features with huge side lobe, hence these features are exacerbated at 6 GHz for both antennas with SRR and at 5 GHz only for T-antenna loaded with SRR (Fig. 5*b*). The huge side lobs can be attributed to the asymmetrical ground planes and the rectangular slots employed for impedance matching. Moreover it is worth mention that, by loading the SRR with asymmetrical meander lines on antennas structures these lobs have great.

The current distribution is most important part to shown the SRR characteristics. Hence, the surface current distributions over the proposed antenna at resonance frequencies are shown in Figs. 5*c* and *d*. The SRR affect the current flow over the antennas to generate the radiation patterns shown in Figs. 5*a* and *b* that are stable across their operating frequency ranges.

As previously mentioned, to validate the design processes, the antennas were modelled and designed by applying Ansoft's 3D full-wave electromagnetic field software, that is, HFSS [23] and after achieving the good simulation results, the antennas were fabricated and tested. The antenna measured data such as bandwidths, gains, efficiencies and radiations patterns were obtained in the antenna and microwave laboratories by network analyser. The measured results of both proposed antennas without/with asymmetrical meander lines SRR loading are summarised in Table 2.

From figures and tables it can be expressed that by applying the asymmetrical meander lines SRR loading, the proposed antennas with approximately same in size exhibits the better operational performances including the broader bandwidths (more than two times for both antennas), higher gains and efficiencies accompanying the improved radiation patterns, curves and current distributions in comparison to antennas designed without SRR loading. Consequently, in achieving better performances compared with conventional versions the SRRs have been loaded onto the conventional unloaded antennas. These loading excite the lower resonance frequencies modes that match with the resonance frequencies of monopole antennas, thereby extending the overall impedance bandwidths from 31.5 to 75.4% (~2.4 times more) for F-antenna and from 41.16 to 86.9% (2.11 times more) for T-antenna. As a result, the second versions with the asymmetrical meander lines SRR loading can be applicable for the WiMAX (3.5–5.5 GHz) and WLAN (5.2–5.8 GHz) bands.

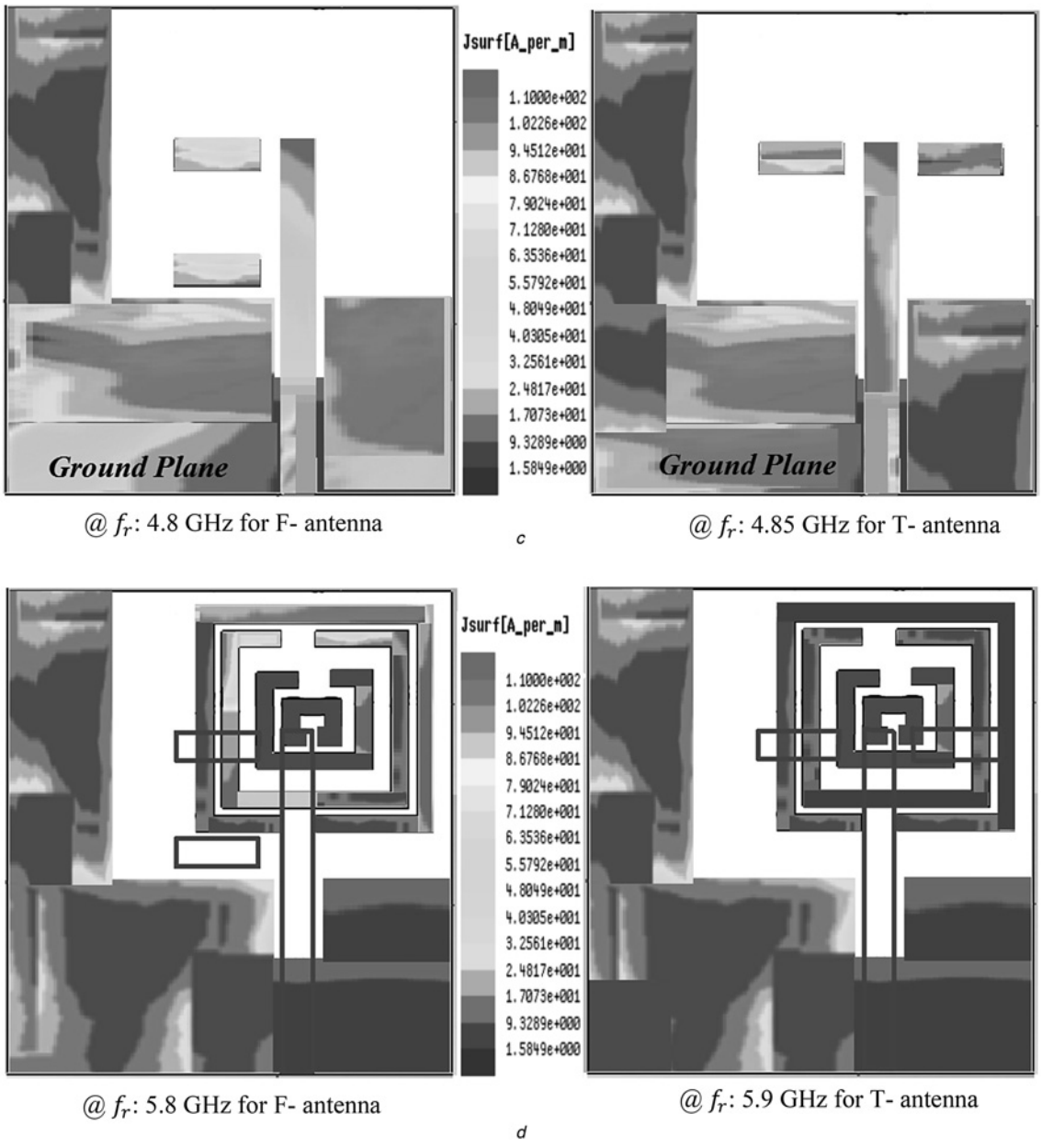

Fig. 5 *Continued*

Hence, effects of asymmetrical meander lines SRRs loading onto the conventional monopole antennas are elaborated in next section.

4 Investigation on effects of asymmetrical meander lines SRR loading

Let us now focus on the propagation characteristics of the proposed structures through the analysis of the dispersion relations. This is inferred from the lumped elements equivalent circuit (Fig. 6), which is valid in the long-wavelength regime ($\beta l \ll 1$, where β is the propagation constant for guided waves).

L and C are the per-section inductance and capacitance of the structures. These parameters model the inductance associated with the central conductor of the structures and the capacitive coupling between these structures and ground planes (slot capacitance), respectively. SRRs are modelled as parallel resonant circuits (with inductance L_S and capacitance C_S) which are inductively coupled to the structure through a mutual inductance, M. After some calculation, the dispersion relation has been found to be

Table 2 Overall characteristics of the proposed antennas

Parameters	F-Ant. without SRR	F-Ant. with SRR	T-Ant. without SRR	T-Ant. with SRR
dimensions	$25 \times 10^{-2}\lambda_0 \times 11 \times 10^{-2}\lambda_0$ @ 4 GHz	$29 \times 10^{-2}\lambda_0 \times 21 \times 10^{-2}\lambda_0$ @ 2.9 GHz	$25 \times 10^{-2}\lambda_0 \times 21 \times 10^{-2}\lambda_0$ @ 4 GHz	$29 \times 10^{-2}\lambda_0 \times 21 \times 10^{-2}\lambda_0$ @ 2.9 GHz
BW	4–5.5 GHz (31.5%)	2.9–6.41 GHz (75.4%) **~2.4 Times More**	3.82–5.8 GHz (41.16%)	2.6–6.6 GHz (~87%) **2.11 Times More**
Max. Ga.	3.6 dBi @ 5 GHz	4 dBi @ 6 GHz	3.9 dBi @ 5 GHz	4.4 dBi @ 6 GHz
Max. Eff.	78.5% @ 5 GHz	81.2% @ 6 GHz	80.2% @ 5 GHz	82.6% @ 6 GHz

IET Microw. Antennas Propag., 2015, Vol. 9, Iss. 14, pp. 1487–1496

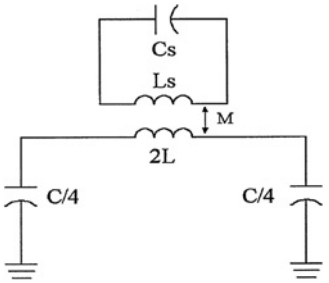

Fig. 6 *Lumped element equivalent circuit for the proposed structures*

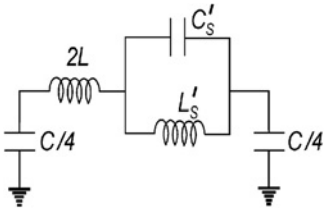

Fig. 7 *Simplified circuit with the series branch replaced by its equivalent impedance*

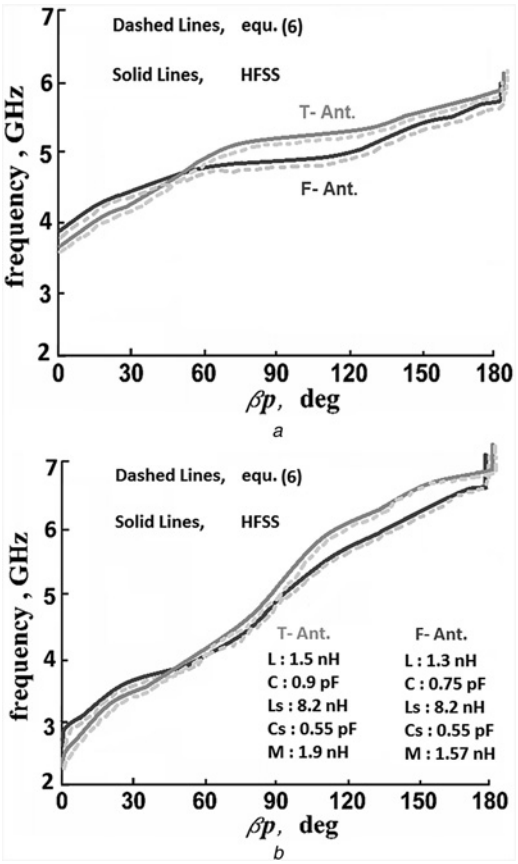

Fig. 8 *Dispersion diagrams of the proposed F- and T-shaped antennas (Blue lines are for F-antenna and Green lines are for T-antenna)*

a Without SRR loading
b Loaded with SRR

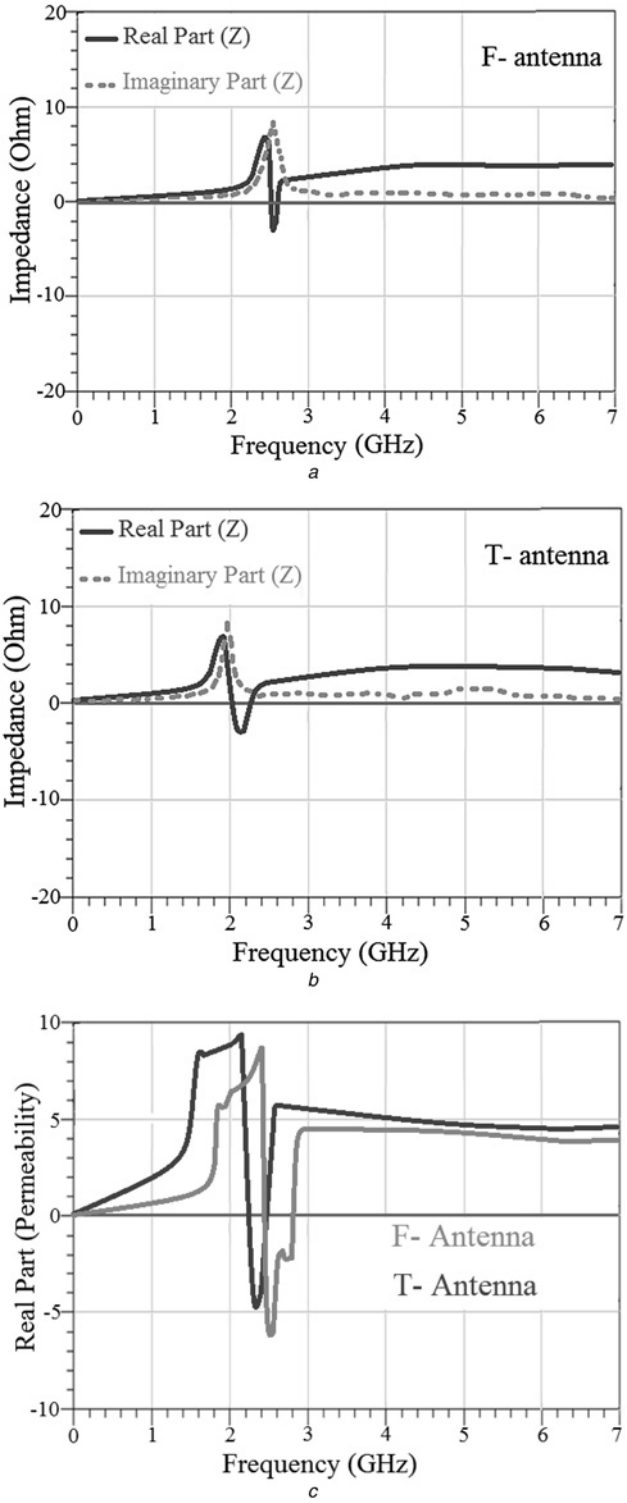

Fig. 9 *Impedance and permeability plots against frequency for proposed antennas loaded with SRR*

a Impedance plots of SRR versus frequency for F-antenna
b Impedance plots of SRR versus frequency for T-antenna
c Permeability Curves of SRR versus frequency for both antennas

$$\cos(\beta l) = 1 - \frac{LC\omega^2}{2} + \frac{(C/C_S')}{4\left(1 - \left[\omega_0^2/\omega^2\right]\right)} \tag{1}$$

$$C_S' = \frac{L_S}{M^2\omega_0^2} \tag{2}$$

$$L_S' = C_S M^2 \omega_0^2 \tag{3}$$

$$\omega_0^2 = \frac{1}{(L_S\, C_S)} = \frac{1}{(L_S' C_S')}. \tag{4}$$

Moreover, M can be inferred from the fraction f of the slot area occupied by the rings according to

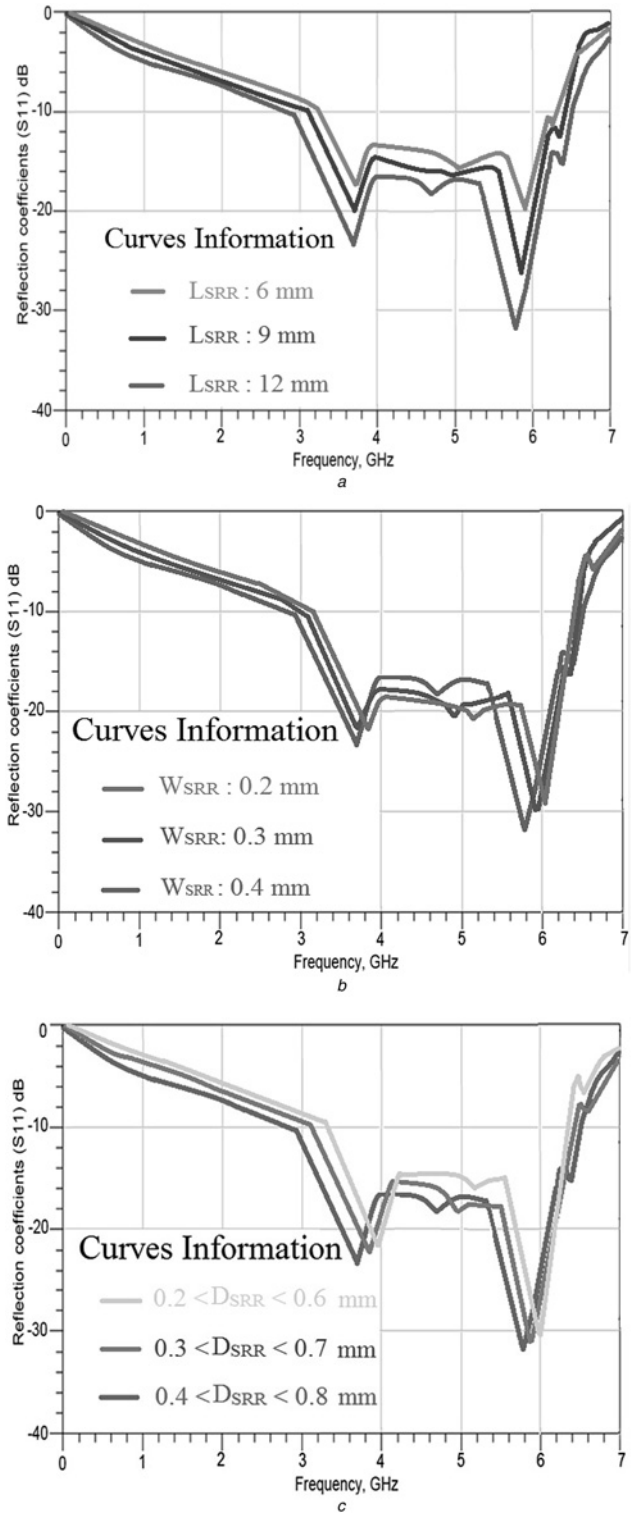

Fig. 10 *Parametric study on SRR dimensions for F-shaped antenna*

a Effects of different lengths (L_S) of SRR on reflection coefficient (The other parameters remain constant)

b Effects of different widths (W_S) of SRR on reflection coefficient (The other parameters remain constant)

c Effects of variation in distances between rings of SRR (D_{SRR}) on reflection coefficient (The other parameters remain constant). The number of SRR pairs is 4, hence distances between the rings are not equal to one. They are variable and their optimal values are in the range of 0.4 mm < D_{SRR} < 0.8 mm

$$M = 2L.f. \tag{5}$$

By obtaining the equivalent impedance of the series branch, the circuit can be simplified to that shown in Fig. 7.

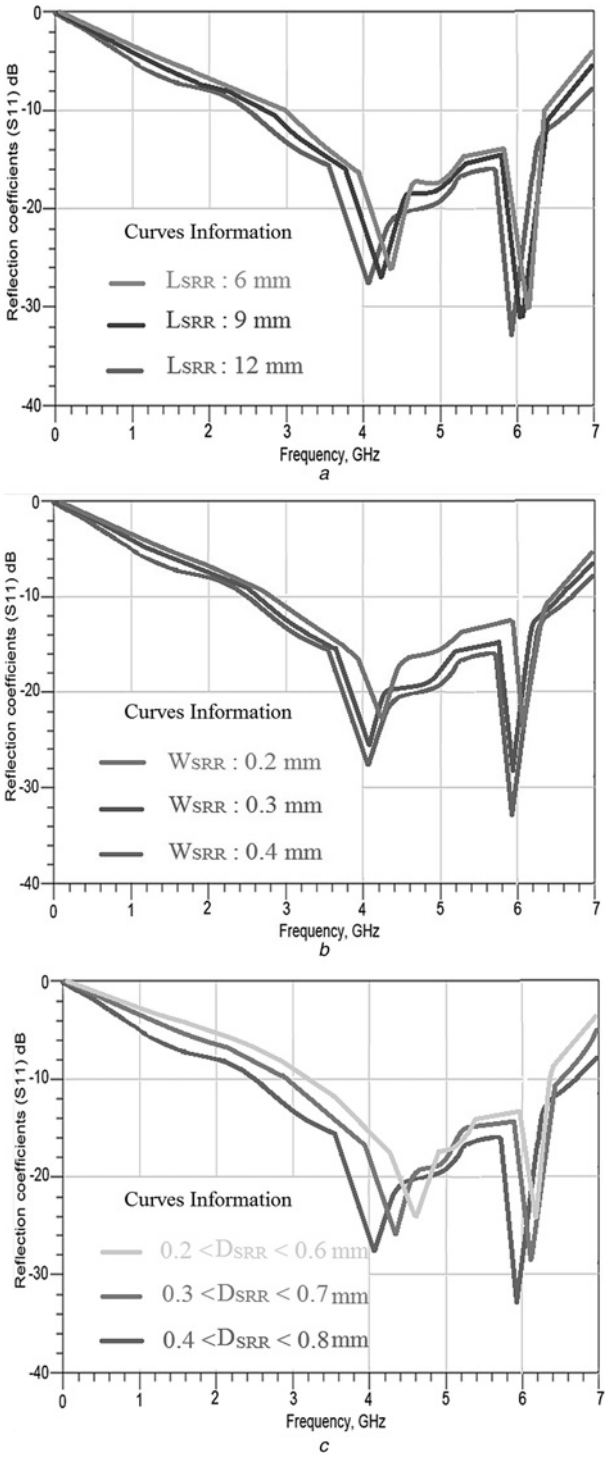

Fig. 11 *Parametric study on SRR dimensions for T-shaped antenna*

a Influences of different lengths (L_S) of SRR on reflection coefficient (The other parameters remain constant)

b Influences of different widths (W_S) of SRR on reflection coefficient (The other parameters remain constant)

c Influences of variation in distances between rings of SRR (D_{SRR}) on reflection coefficient (The other parameters remain constant). The number of SRR pairs is 4, hence distances between the rings are not equal to one. They are variable and their optimal values are in the range of 0.4 mm < D_{SRR} < 0.8 mm

The dispersion relation for the circuit of Fig. 7 can be easily obtained from standard calculus [24]

$$\cos(\beta l) = 1 - \frac{L\omega - (1/C\omega)}{(4L/C)}\left[2L\omega - \frac{(L'_S/C'_S)}{L'_S\omega - (1/C'_S\omega)}\right] \tag{6}$$

IET Microw. Antennas Propag., 2015, Vol. 9, Iss. 14, pp. 1487–1496

The dispersion diagrams for the corresponding structures using HFSS and (6) are depicted in an ω–β diagram in Fig. 8. The circuit elements have been calculated for the structures shown in Fig. 2 (the pairs of SRRs are placed in the back substrate side). As can be seen, by loading SRRs on the proposed structures their impedance bandwidths have enhanced.

To validate the results of both proposed antennas, asymmetrical meander lines SRR simulated specifications are expressed. SRR characteristics are studied by Ansys HFSS simulation tool. The effective medium theory has applied to calculate the permeability of SRR. Nicolson–Ross–Weir method was used to obtain the permeability of SRR [25]. Impedance and permeability curves of SRR for F- and T-shaped antennas are plotted in Figs. 9*a*–*c*, respectively. As seen in Figs. 9*a*–*c*, the impedance and permeability of SRR for both antennas are positive and stable in the operating bands of antennas [13, 26].

To providing the desired performances, the dimensions of the asymmetrical meander lines SRR have optimised and regulated using Ansys HFSS EM simulator. Figs. 10 and 11 explain the effects of SRR dimensions on the reflection coefficients ($S_{11} < -10$ dB) of the proposed antennas for various lengths (L_{SRR}), widths (W_{SRR}) and distances between rings of SRR (D_{SRR}).

As observed from Figs. 10 and 11, when the lengths (L_{SRR}), widths (W_{SRR}) and distances between rings of SRR (D_{SRR}) for both antennas increase the negative permeability characteristics of SRR accompanying the resonant frequencies of antennas are slightly shifted to lower frequencies and consequently extension in the antennas bandwidths is observed (7).

$$\mu = L'_{S} - \frac{1}{\omega^2 C'_{S}} \tag{7}$$

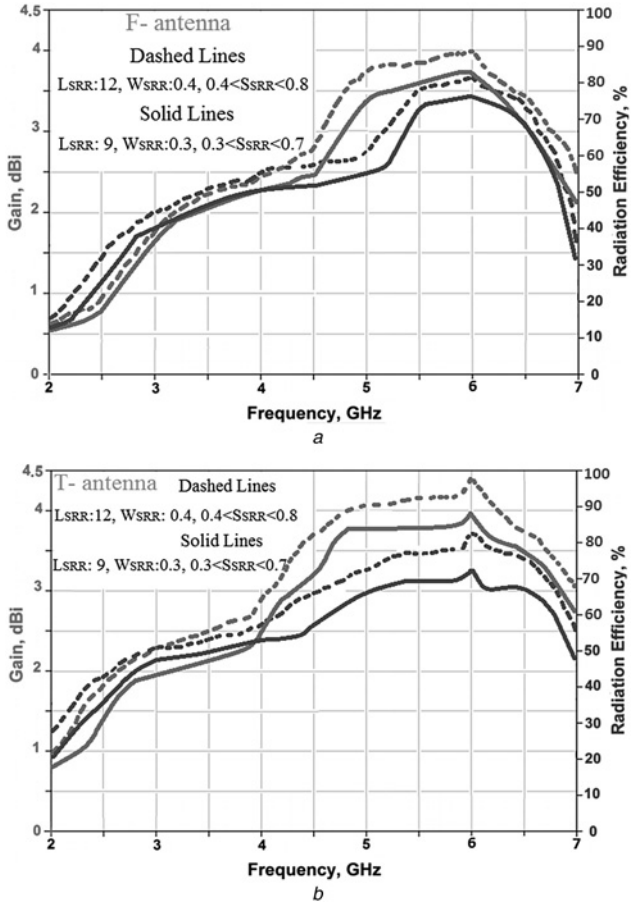

Fig. 12 *Parametric study on the radiation characteristics of proposed antennas by different dimensions of SRR against frequency*

a For F-shaped antenna
b For T-shaped antenna

Besides investigations on bandwidths of antennas by variations of SRR dimensions, a parametric study by SRR on the radiation specifications of the proposed antennas too is studied (Figs. 12*a* and *b*).

Figs. 12*a* and *b* express that, by increasing the dimensions of SRR loaded on the antennas the gains and efficiencies of them have improved on the entire frequency bandwidths.

5 Conclusions

Two antennas in different configurations with/ without SRR loading have been designed, constructed, and tested. The broader bandwidth along with better radiation characteristics were obtained by SRR loading on the conventional unloaded monopole antennas. The SRR loaded antennas excite a lower resonance frequency mode that matches with the resonance frequency of the monopoles, thereby extending the overall impedance bandwidths from 31.5% to 75.4% (~2.4 times more) for F-antenna and from 41.16 to 86.9% (2.11 times more) for T-antenna. The proposed loaded antennas have the small size of $29 \times 10^{-2}\lambda_0 \times 21 \times 10^{-2}\lambda_0$ both at 2.9 GHz. The maximum values of the measured gain and efficiency for F- and T-shaped antennas with the SRR loading appear at operating frequency of 6 GHz that are 4 dBi and 81.2%, and 4.4 dBi, and 82.6%, respectively. Hence, by applying SRR loading, the second versions of antennas can be applicable for WiMAX band (3.5–5.5 GHz) and WLAN band (5.2–5.8 GHz), offering good gains and efficiencies through the whole frequency bandwidths.

6 References

1 Jee, Y., Seo, Y.M.: 'Triple-band CPW-fed compact monopole antennas for GSM/PCS/DCS/WCDMA applications', *Electron. Lett.*, 2009, **45**, (9), pp. 446–448
2 Jo, S., Choi, H., Shin, B., Oh, S., Lee, J.: 'A CPW-Fed rectangular ring monopole antenna for WLAN applications', *Int. J. Antennas Propag.*, 2014, **2014**, article id 9519, 6 pages, doi: 10.1155/2014/951968
3 Anguera, J., Andújar, A., Huynh, M.C., Orlenius, C., Picher, C., Puente, C.: 'Advances in antenna technology for wireless handheld devices', *Int. J. Antennas Propag.*, 2013, **2013**, article id 838364, 25 pages
4 Zuo, S., Yin, Y., Zhang, Z., Wu, W.: 'A compact tri-band PIFA antenna for WLAN and WiMAX applications', *Microw. Opt. Technol. Lett.*, 2010, **52**, (4), pp. 919–922
5 Lee, C.T., Wong, K.L.: 'Uniplanar printed coupled-fed PIFA with a band-notching slit for WLAN/WiMAX operation in the laptop computer', *IEEE Trans. Antennas Propag.*, 2009, **57**, (4), pp. 1252–1258
6 Jofre, L., Cetiner, B.A., De Flaviis, F.: 'Miniature multi-element antenna for wireless communications', *IEEE Trans. Antennas Propag.*, 2002, **50**, pp. 658–669
7 Alibakhshi Kenari, M.: 'Printed planar patch antennas based on metamaterial', *Int. J. Electron. Lett.*, 2014, **2**, (1), pp. 37–42
8 Lai, A., Caloz, C., Itoh, T.: 'Composite right/left-handed transmission line metamaterials', *IEEE Microw. Mag.*, 2004, **5**, (3), pp. 34–50
9 Lee, C.J., Leong, K.M.K.H., Itoh, T.: 'Composite right/left-handed transmission line based compact resonant antennas for RF module integration', *IEEE Trans. Antennas Propag.*, 2006, **54**, (8), pp. 2283–2291
10 Engheta, N., Ziolkowski, R.W. (Eds): 'Metamaterials: physics and engineering explorations' (Wiley-IEEE Press, New York, NY, USA, 2006, 440 pages)
11 Caloz, C., Itoh, T.: 'Electromagnetic metamaterials: transmission line theory and microwave applications, the engineering approach' (John Wiley & Sons, New York, 2005, 376 pages)
12 Caloz, C., Itoh, T., Rennings, A.: 'CRLH metamaterial leaky-wave and resonant antennas', *IEEE Antennas Propag. Mag.*, 2008, **50**, (5), pp. 25–39
13 Alu, A., Bilotti, F., Engheta, N., Vegni, L.: 'Sub-wavelength, compact, resonant patch antennas loaded with metamaterials', *IEEE Trans. Antennas Propag.*, 2007, **55**, (1), pp. 13–25
14 Sanada, A., Caloz, C., Itoh, T.: 'Zeroth order resonance in the left-handed transmission line', *IEICE Trans. Electron.*, 2004, **87-C**, (1), p. 17
15 Caloz, C., Itoh, T.: 'Novel microwave devices and structures based on the transmission line approach of meta-materials'. IEEE Int. Symp. on Microwave Theory and Techniques Digest, Philadelphia, USA, June 2003, pp. 195–198
16 Schussler, M., Freese, J., Jakoby, R.: 'Design of compact planar antenna using LH-transmission lines'. IEEE MTT-S Int. Microwave Symp., June 2004, vol. 1, pp. 209–212
17 Alibakhshi-Kenari, M.: 'Introducing the new wide band small plate antennas with engraved voids to form new geometries based on CRLH MTM-TLs for wireless applications', *Int. J. Microw. Wirel. Tech.*, 2014, **6**, (Special Issue 6), pp. 629–637
18 Abdollahvand, M., Dadashzadeh, G., Mostafa, D.: 'Compact dualband-notched printed monopole antenna for UWB application', *IEEE Antennas Wirel. Propag. Lett*, 2010, **9**, pp. 1148–1151

19 Lee, C.J., Leong, K.M.H., Itoh, T.: 'Broadband small antenna for portable wireless application'. Int. Workshop on Antenna Technology: Small Antennas and Novel Metamaterials, iWAT 2008, 4–6 March 2008, pp. 10–13
20 Alibakhshi-Kenari, M.: 'A new compact UWB traveling-wave antenna based on CRLH-TLs for embedded electronic systems', *Int. J. Microw. Wireless Tech.*, 2014, pp. 1–4, doi: http://dx.doi.org/10.1017/S1759078714001020
21 Wu, S.J., Kang, C.H., Chen, K.H., Tarng, J.H.: 'Study of an ultra wideband monopole antenna with a band-notched open-looped resonator', *IEEE Trans. Antennas Propag.*, 2010, **58**, (6), pp. 1890–1897
22 Movahedinia, R., Azarmanesh, M.N.: 'A novel planar UWB monopole antenna with variable frequency band-notch function based on etched slot-type ELC on the patch', *Microw. Opt. Technol. Lett.*, 2010, **52**, (1), pp. 229–232
23 Ansoft HFSS www.ansoft.com/products/hf/hfss
24 Pozar, M.: 'Microwave Engineering' (Addison–Wesley, Reading, MA, 1993)
25 Ziolkowski, R.W.: 'Design, fabrication, and testing of double negative metamaterials', *IEEE Trans. Antennas Propag.*, 2003, **51**, pp. 1516–1529
26 Ikonen, P.M.T., Maslovski, S.I., Simovski, C.R., Tretyakov, S.A.: 'On artificial magnetodielectric loading for improving the impedance bandwidth properties of microstrip antennas', *IEEE Trans. Antennas Propag.*, 2006, **54**, pp. 1654–1662